Supplementary Figures

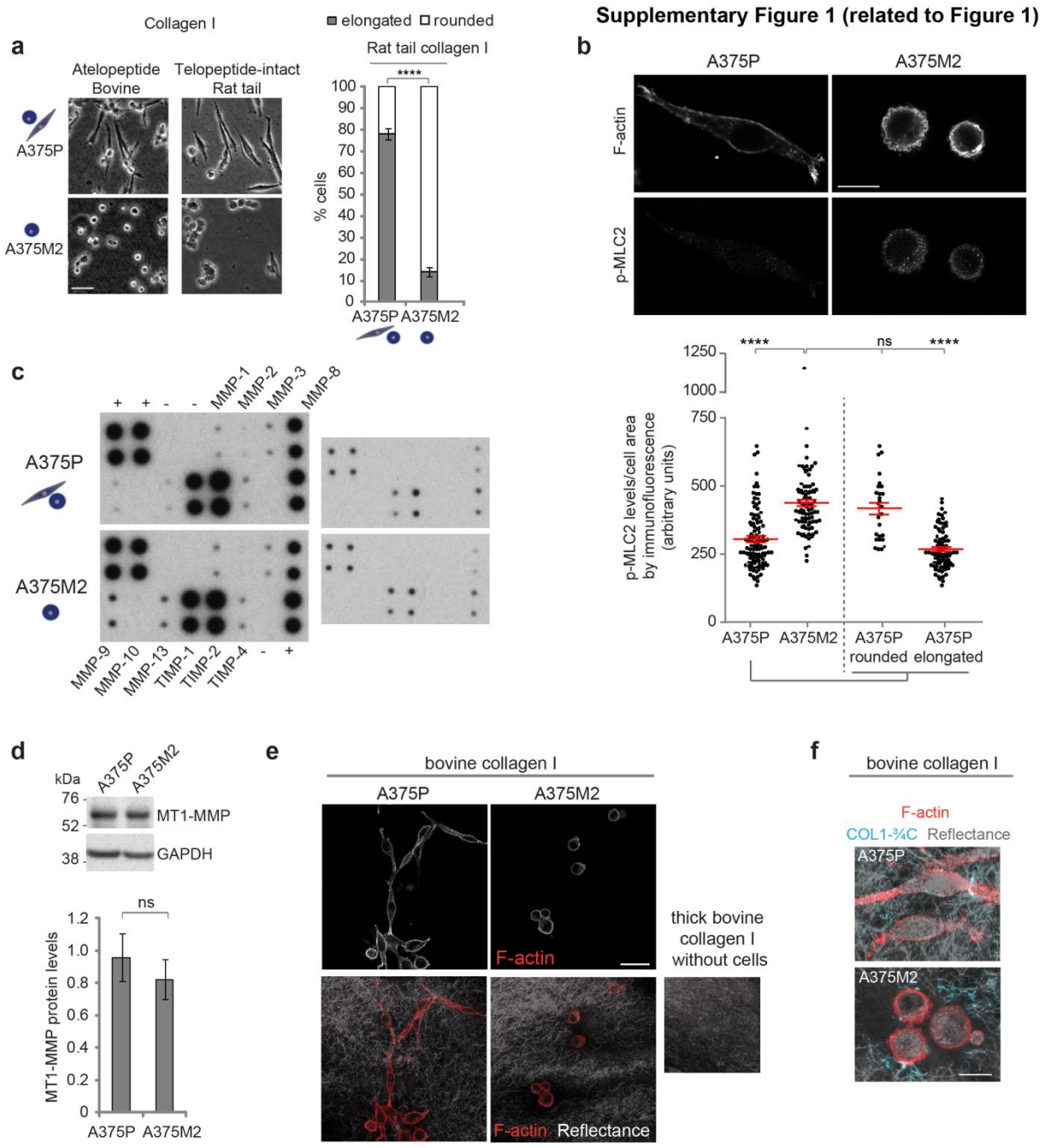

Supplementary Figure 1. Rounded-amoeboid cells produce MMPs on collagen matrices (related to Figure 1). (**a**) Representative bright-field images of A375P and A375M2 cells on top of atelopeptide (bovine) and telopeptide-intact (rat tail) collagen I. Scale bar, 50 µm. (left). Percentage of rounded and elongated A375P and A375M2 cells on top of telopeptide-intact (rat tail) collagen I (manual classification) (600 cells/experiment, n=4) (right). (**b**) Representative confocal images (top) and quantification (bottom) of phospho-MLC2 (p-MLC2) immunostaining in A375P and A375M2 cells on bovine collagen I. F-actin staining is also shown. Dots represent single cells from 2 independent experiments. Scale bar, 25 µm. (**c**) Protein array with all the MMPs and TIMPs labelled for each dot. Dots in the upper left and lower right corners serve as loading controls. Right panels show different exposures of the MMP array. (**d**) Representative MT1-MMP immunoblot (top) and protein levels (bottom) in A375M2 and A375P cells (n=4). (**e**) Confocal images of A375P and A375M2 cells on bovine collagen I. F-actin (red) staining is shown. ECM fibers are detected from backscattered light/reflectance (grey). Collagen I without cells is also shown. Scale bar, 50 µm. (**f**) Confocal images of collagen cleavage neo-epitope COL1-¾C (cyan) immunostaining within 10 µm from edge of A375P and A375M2 cells on bovine collagen I. F-actin (red) and reflectance (grey) are also shown. Scale bar, 25 µm.

Graphs show mean ± s.e.m. *p<0.05, **p< 0.01, ***p<0.001, ****p<0.0001, ns not significant. Unpaired t-test (a, d), ANOVA with Tukey's post hoc test (b).

Supplementary Figure 2 (related to Figure 2)

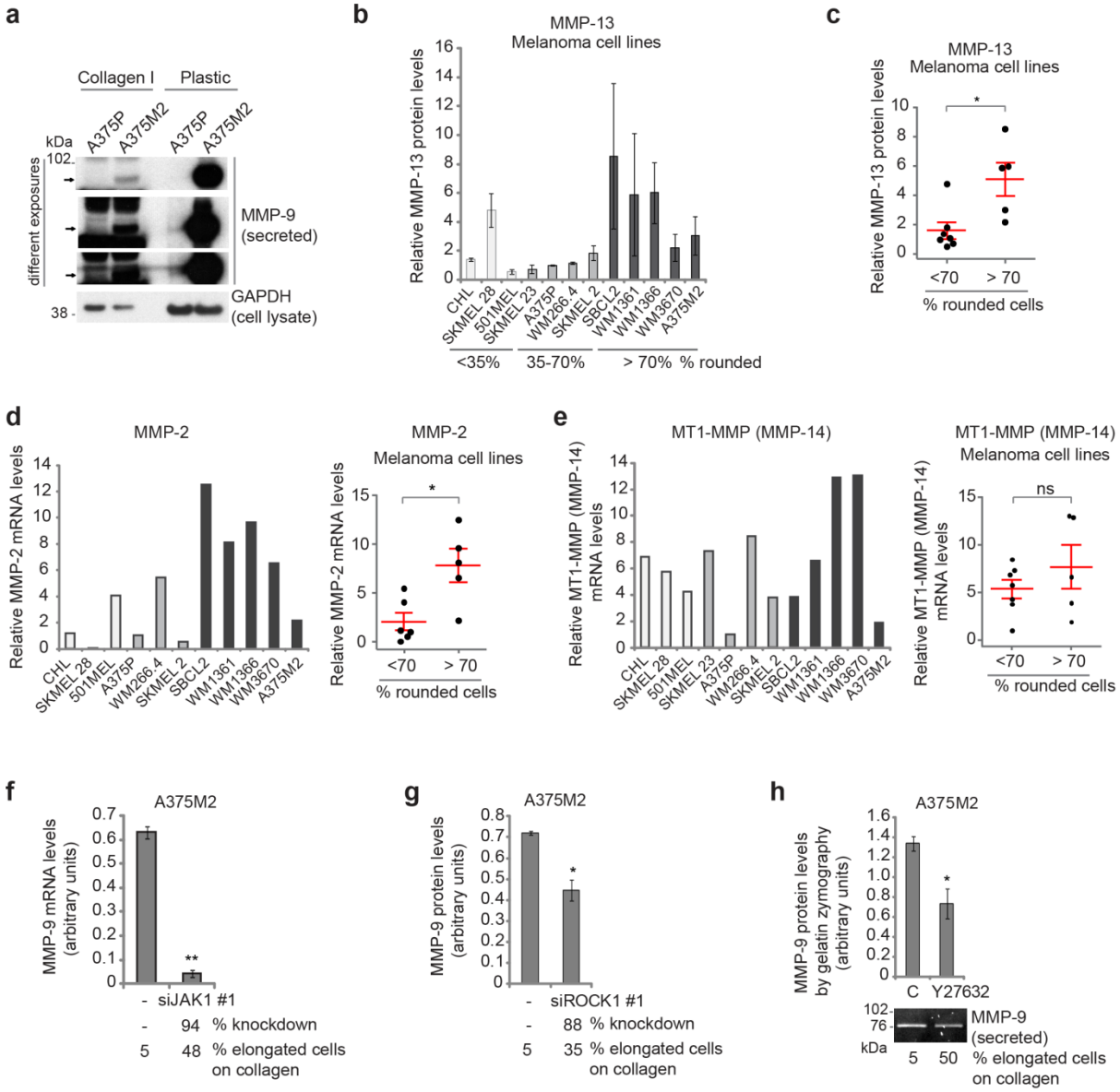

Supplementary Figure 2. ROCK-JAK-STAT3 regulate MMP-9 in rounded-amoeboid cells (related to Figure 2). (**a**) Immunoblot of secreted MMP-9 from A375P and A375M2 cells on top of bovine collagen and plastic. GAPDH from cell lysates is also shown. Different exposures of MMP-9 blot are displayed. (**b**) Secreted MMP-13 protein levels by immunoblot in a panel of melanoma cell lines (relative to A375P =1) (n=3). (**c**) Relative MMP-13 protein levels in the panel of melanoma cell lines from (b) grouped as mostly elongated (<70% rounded cells) or mostly rounded (>70% rounded cells). (**d**) MMP-2 mRNA expression levels in a panel of melanoma cell lines (left, relative to A375P) and in the same cell lines grouped (right) as mostly elongated (<70% rounded cells) or mostly rounded (>70% rounded cells). (**e**) MT1-MMP (MMP-14) mRNA expression levels in a panel of melanoma cell lines (left, relative to A375P) and in the same cell lines grouped (right) as mostly elongated (<70% rounded cells) or mostly rounded (>80% rounded cells). (**f**) MMP-9 mRNA levels in A375M2 cells after JAK1 depletion (n=3). Percentage of JAK1 knockdown by qRT-PCR and percentage of elongated cells on collagen after JAK1 knockdown are shown below graph. (**g**) MMP-9 secreted protein levels in A375M2 cells after ROCK1 depletion (n=3). Percentage of ROCK1 knockdown by qRT-PCR and percentage of elongated cells on collagen are shown below. (**h**) Quantification by gelatin zymography of secreted MMP-9 in A375M2 cells after ROCK inhibitor (Y27632; C=control) treatment for 48 h (n=5). Lower panel: representative gelatin zymography and percentage of elongated cells on collagen after Y27632

treatment. Graphs show mean ± s.e.m. *p<0.05, **p< 0.01, ***p<0.001, ****p<0.0001, ns not significant. Unpaired t-test (c, d, e, f, g, h).

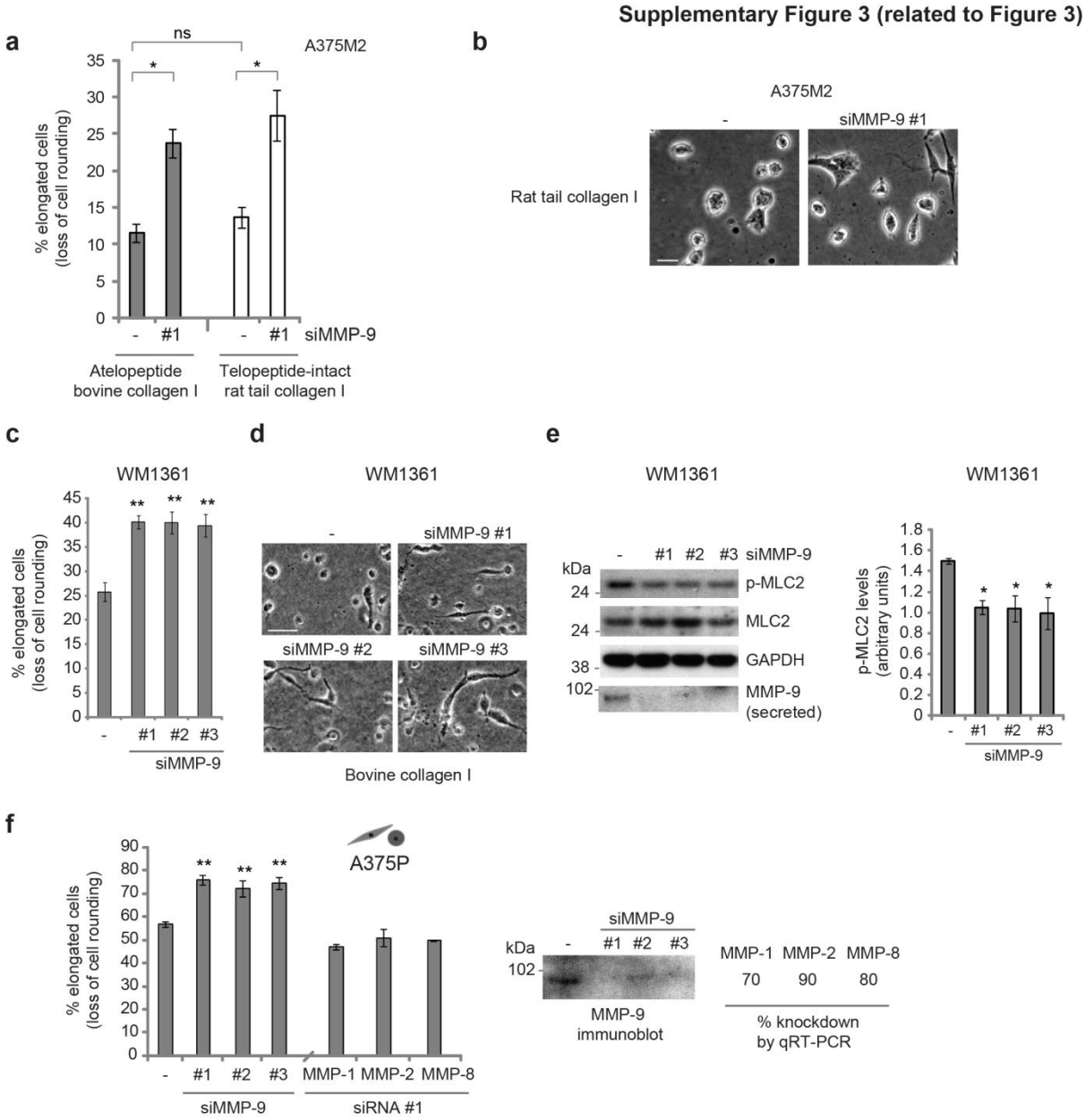

Supplementary Figure 3. MMP-9 positively regulates roundness and MLC2 activity (related to Figure 3). (**a**) Percentage of elongated A375M2 cells on top of atelopeptide bovine and telopeptide-intact rat tail collagen I after MMP-9 knockdown (600 cells/experiment, n=4). (**b**) Representative bright-field images of A375M2 cells on top of rat tail collagen I after MMP-9 knockdown. Scale bar, 50 µm. (**c**) Percentage of elongated WM1361 cells after MMP-9 knockdown (n=5). (**d**) Representative bright-field images of WM1361 cells after MMP-9 knockdown. Scale bar, 50 µm. (**e**) Representative immunoblot (left) and phospho-MLC2 (p-MLC2) levels (right) in WM1361 cells after MMP-9 knockdown (n=5). (**f**) Percentage of elongated A375P cells after MMP-9, MMP-1, MMP-2 and MMP-8 knockdown. MMP-9 immunoblot and the percentage of knockdown by qRT-PCR are also shown. Graphs show mean ± s.e.m. *p<0.05, **p< 0.01, ***p<0.001, ****p<0.0001, ns not significant. ANOVA with Tukey's post hoc test (a, c, e, f).

Supplementary Figure 4 (related to Figure 4)

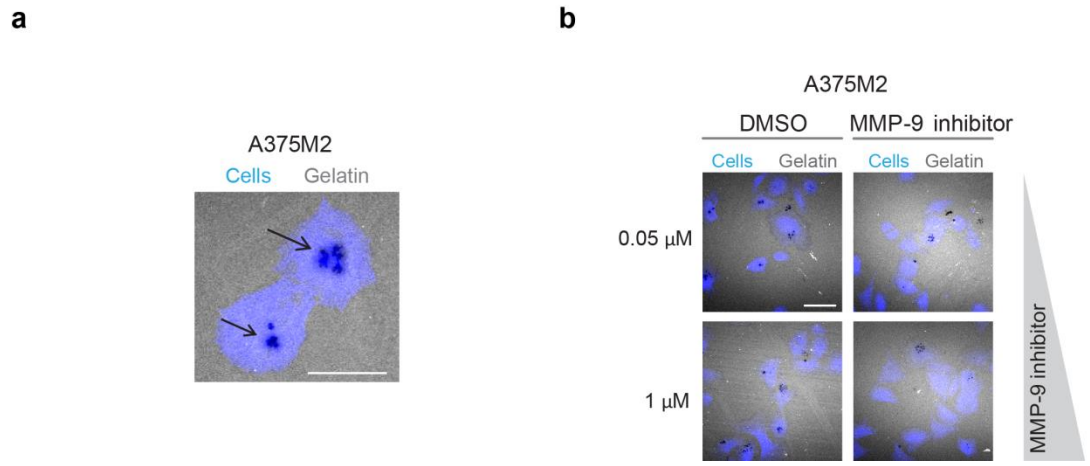

Supplementary Figure 4. MMP-9 function is independent of its catalytic activity (related to Figure 4). Representative confocal images of CMFDA Green-stained A375M2 cells (blue) plated on rhodamine-labelled gelatin (grey) and treated with the indicated concentrations of MMP9 inhibitor I. (**a**) Higher magnification image, arrows point at gelatin degradation spots. Scale bar, 25 µm. (**b**) Lower magnification images. Scale bar, 50 µm.

Supplementary Figure 5 (related to Figure 5)

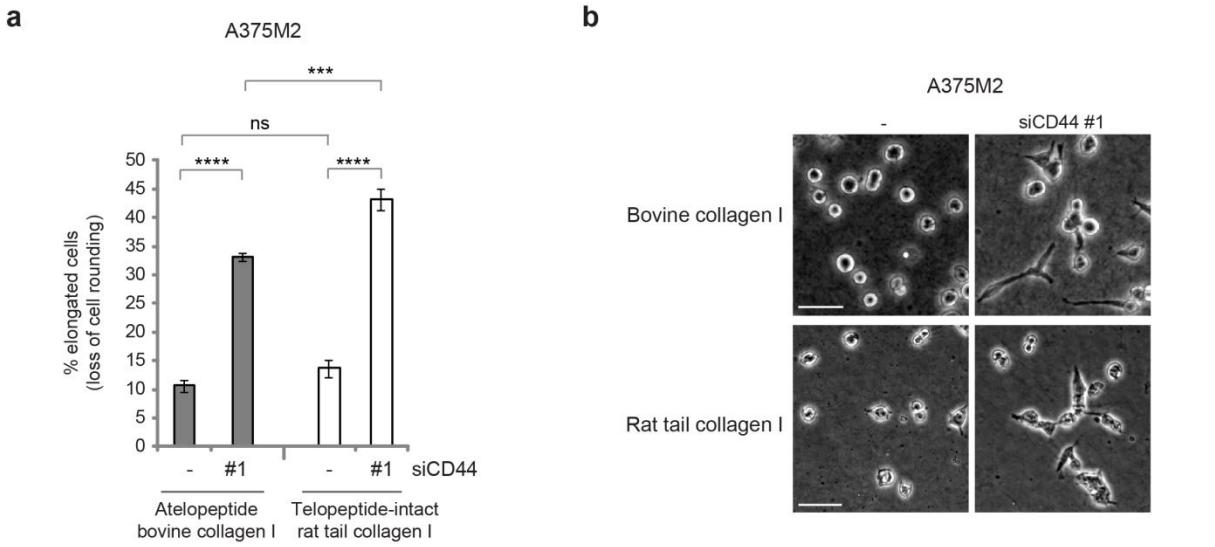

Supplementary Figure 5. MMP-9 regulates rounded-amoeboid migration via CD44 (related to Figure 5). (**a**) Percentage of elongated A375M2 cells on atelopeptide bovine and telopeptide-intact rat tail collagen I after CD44 depletion (n=5). (**b**) Representative bright-field images of A375M2 cells on bovine and rat tail collagen I after CD44 depletion. Scale bar, 50 µm. Graphs show mean ± s.e.m. *p<0.05, **p< 0.01, ***p<0.001, ****p<0.0001, ns not significant. ANOVA with Tukey's post hoc test (a).

Supplementary Figure 6 (related to Figure 6)

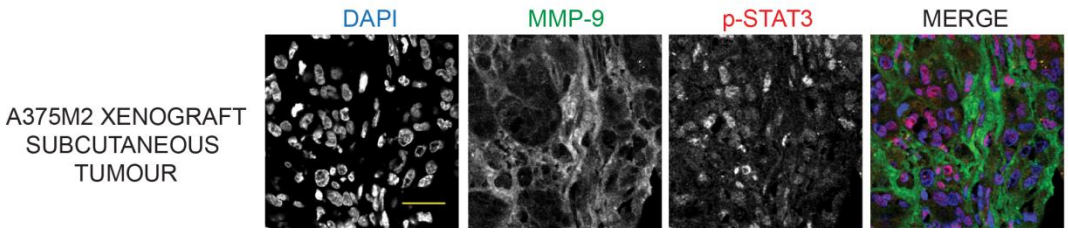

Supplementary Figure 6. MMP-9 from rounded-amoeboid melanoma cells is important in vivo (related to Figure 6). Representative confocal images of invasive front of A375M2 xenograft subcutaneous tumours immunostained for MMP-9 (green) and p-STAT3 (red). Nuclei were stained with DAPI (blue). Scale bar, 35 µm.

Supplementary Figure 7

Figure 1

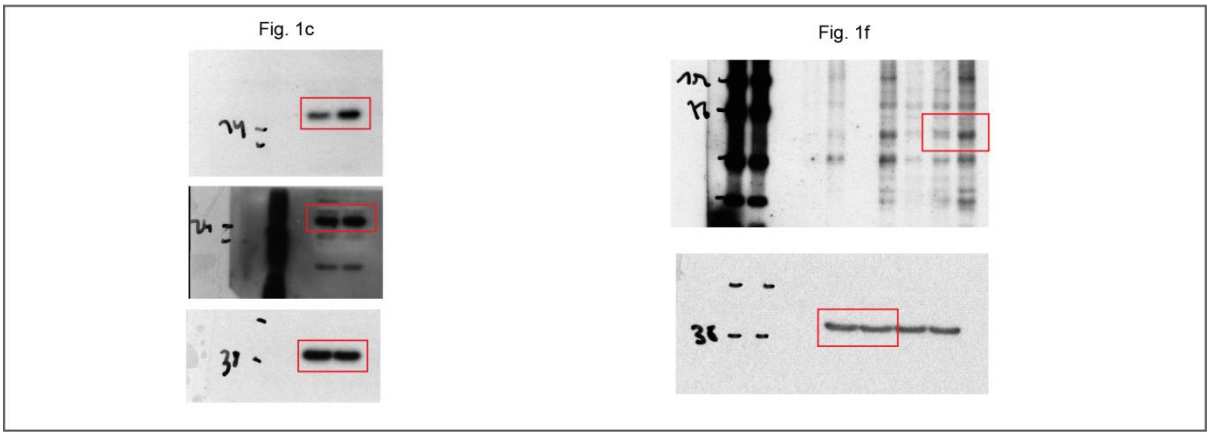

Figure 2

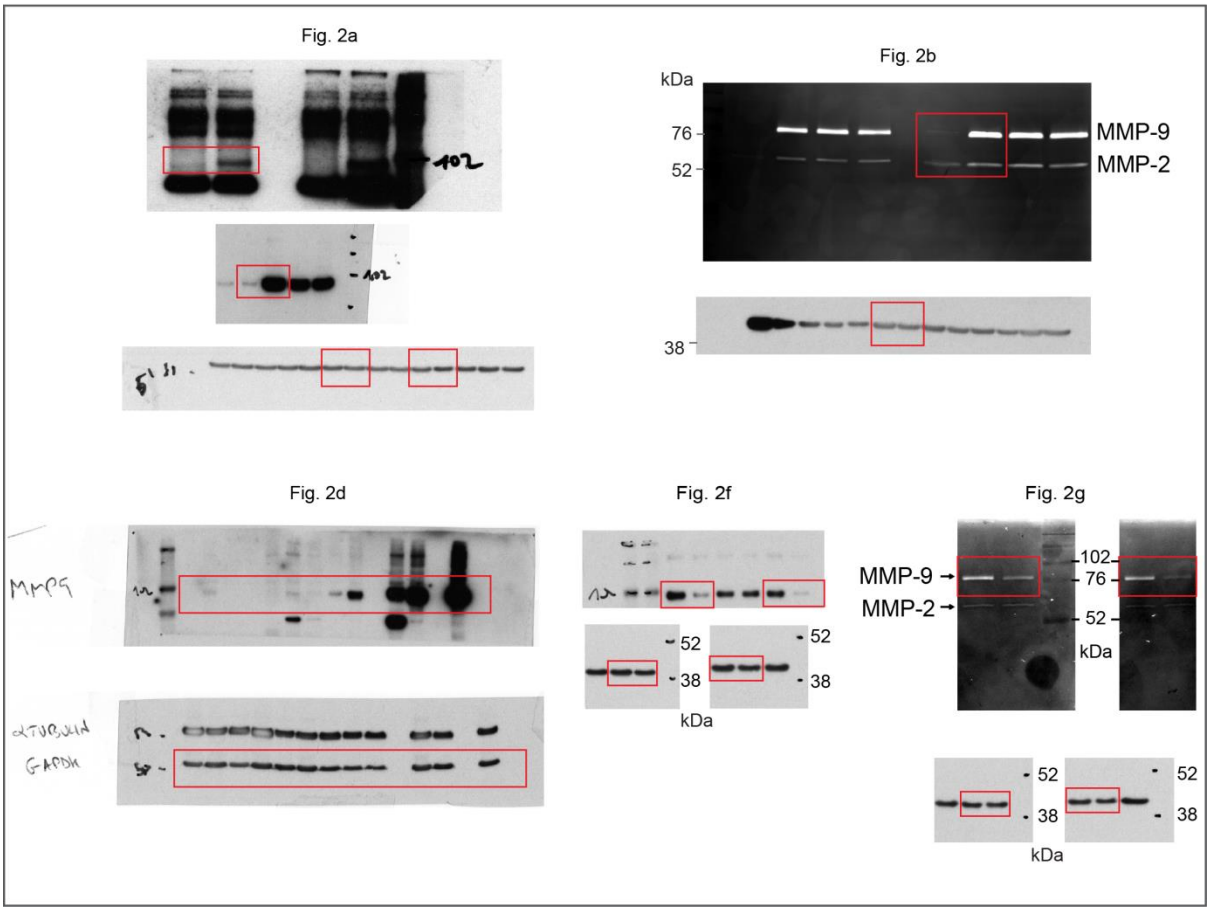

Supplementary Figure 7. Full blots and zymography gels from main figures. Boxes highlight lanes used in figures. Note that in Fig. 2a there are some unspecific bands that do not disappear after RNAi to MMP-9.

Figure 3

Supplementary Figure 8

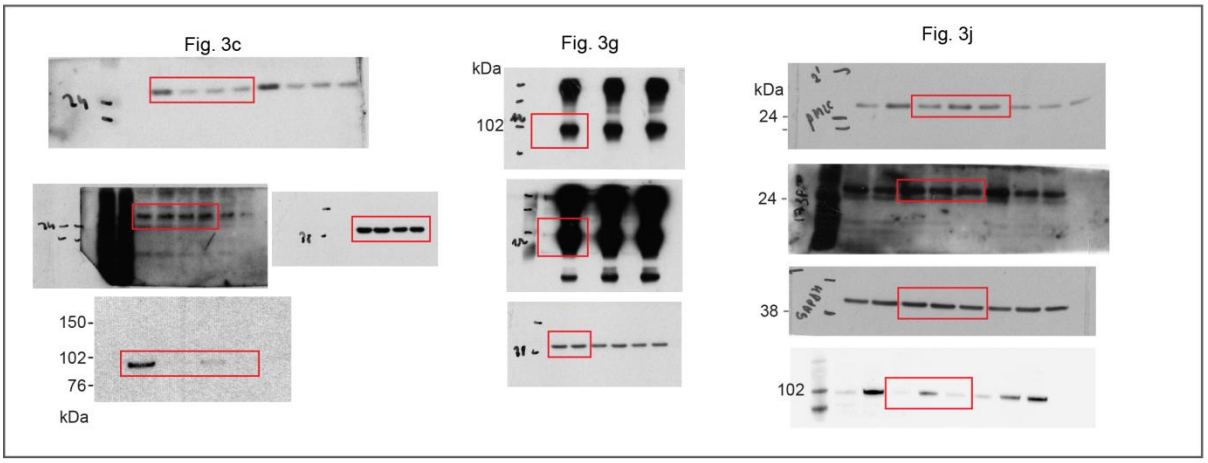

Figure 4

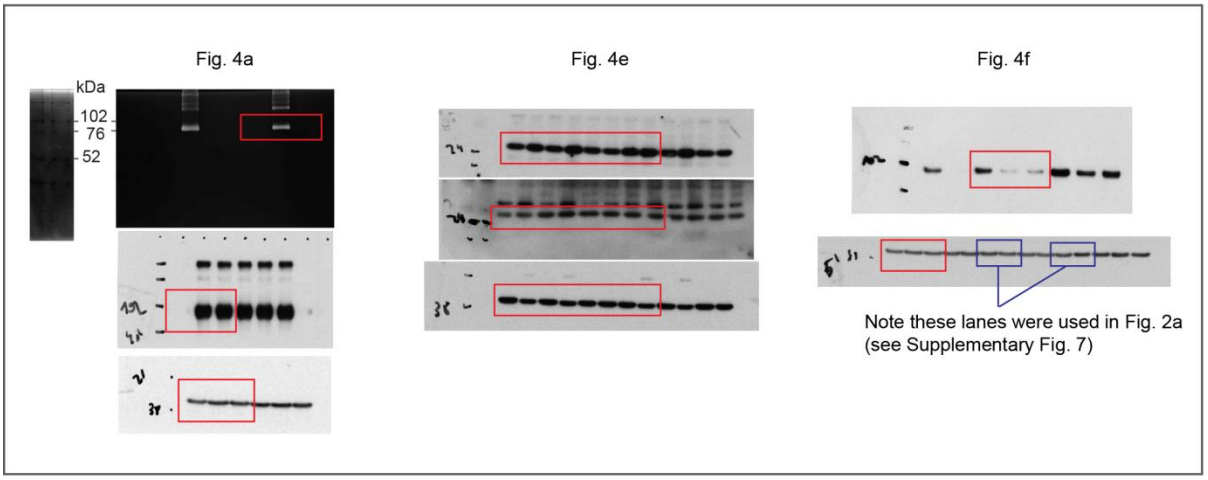

Figure 5

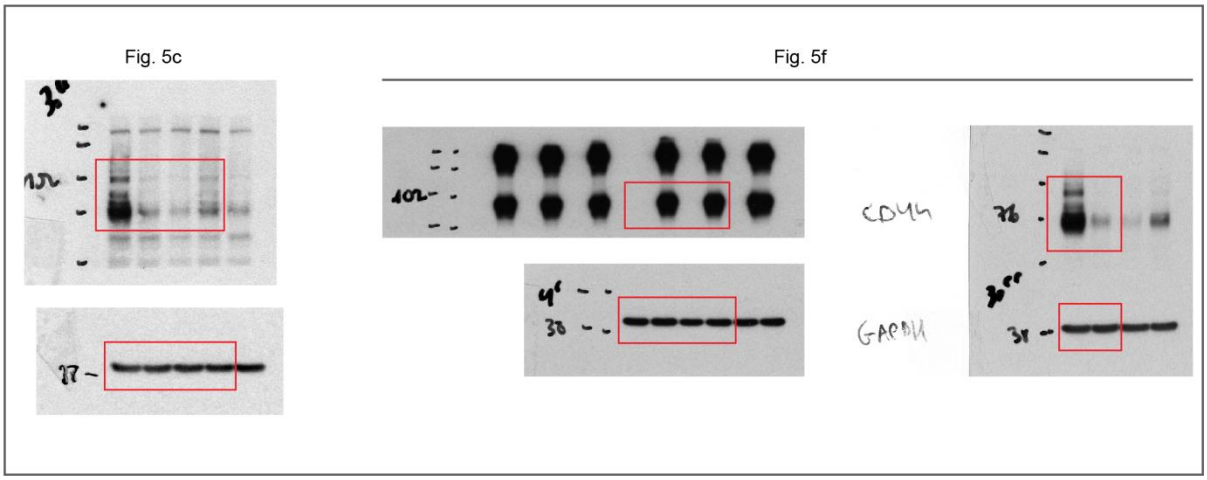

Supplementary Figure 8. Full blots and zymography gels from main figures (continues from Supplementary Fig. 7). Boxes highlight lanes used in figures. Note that in Fig. 4a, only MMP-9 (but not MMP-2) was detected in secreted media from MMP-9-overexpressing HEK293T cells.

Supplementary Table 1

Raw data from the human melanoma patients stained for MMP-9 and p-STAT3.

Patient ID	Gender	Age	Stage	Classification
1	M	55	IV	Subcutaneous metastasis
2	M	72	IV	Distant lymph node metastasis
3	F	55	IV	In transit metastasis
4	M	74	IIIB	Subcutaneous metastasis
5	F	84	IIIB	In transit metastasis
6	N/A	N/A	N/A	Lymph node metastasis
7	N/A	N/A	N/A	Primary melanoma
8	N/A	N/A	N/A	Primary melanoma